energies

MDPI

Article

Research on Online Detection Method of Transformer Winding Deformation Based on VFTO Characteristics

Xinghua Shi [1], Ran Wei [1] and Wenbin Zhang [2,*]

[1] Faculty of Science, Kunming University of Science and Technology, Kunming 650504, China; xinghuashi@kust.edu.cn (X.S.)
[2] College of Mechanical and Electrical Engineering, Kunming University of Science and Technology, Kunming 650504, China
* Correspondence: zwbscg@kust.edu.cn; Tel.: +86-153-0885-9327

Abstract: At present, most of the winding fault detections of transformers use offline methods, which require the entire line to be powered off or after the transformer has been shut down due to a serious fault, and they cannot detect the running status of the windings in real time and online. Since the transformer will be impacted by VFTO during operation, the VFTO is used as the excitation, and the basic principle of the frequency response method is used to propose an online detection method of transformer winding deformation based on VFTO characteristics. The finite element software is used to calculate the equivalent circuit parameters of normal and deformed windings, and the equivalent circuit model of the transformer windings before and after deformation is established. Due to the uncertainty of the VFTO waveform, combined with the frequency response method, the VFTO waveform is injected into the transformer winding health, and the frequency response curve is obtained from the deformed equivalent circuit, which is used to analyze the change of the resonance point in the case of radial deformation, axial deformation, and axial displacement of the winding. The simulation results show that with VFTO as the excitation, the obtained resonance point change can comprehensively reflect the deformation information of the winding. At the same time, the feasibility of the method is verified by experiments.

Keywords: transformer winding; winding deformation; frequency response method; VFTO characteristics

check for updates

Citation: Shi, X.; Wei, R.; Zhang, W. Research on Online Detection Method of Transformer Winding Deformation Based on VFTO Characteristics. *Energies* **2023**, *16*, 3496. https://doi.org/10.3390/en16083496

Academic Editor: Adolfo Dannier

Received: 10 March 2023
Revised: 14 April 2023
Accepted: 14 April 2023
Published: 17 April 2023

Copyright: © 2023 by the authors. Licensee MDPI, Basel, Switzerland. This article is an open access article distributed under the terms and conditions of the Creative Commons Attribution (CC BY) license (https://creativecommons.org/licenses/by/4.0/).

1. Introduction

Failure types of transformers include oil leakage, casing failure, poor core insulation and ground connection, damaged winding insulation, etc. [1]. Referring to the statistics of relevant departments, winding faults account for 40.22% of the total number of other faults and have been increasing in recent years [2]. External short-circuit fault is the most important cause of transformer winding distortion. The interaction between the short-circuit current and the magnetic field inside the transformer will produce a large short-circuit force. Short-circuit forces have components in both radial and axial directions; that is, radial and axial stresses. Different stresses result in different transformer failures [3]. The radial force tends to stretch the conductor, while the external winding tends to collapse or destroy the internal winding. Axial force acting on the winding will destroy the conductor insulation by axially passing through adjacent wires, which will eventually cause turn-to-turn failures and even power supply interruptions and electrical equipment outages. As the core component of the power system, the transformer cannot be in power failure for a long time. It is very important to detect winding distortion before transformer failure. Currently, most of the transformer winding inspection work is carried out offline.

There are currently mature methods for offline detection of transformer winding faults, such as the short-circuit impedance method and the frequency response method [4,5]. The short-circuit impedance method can be used to determine if the transformer windings are deformed by comparing the short-circuit impedance of the transformer with the data

before the transformer starts to operate. Although the short-circuit impedance calculation is simple, it has low sensitivity and a high probability of misjudgment. When short-circuit impedance is tested, it needs to work with various test equipment, which is labor-intensive and takes a long time to complete.

Frequency response methods can be divided into impulse frequency response analysis (IFRA) and sweep frequency response analysis (SFRA). IFRA uses a pulse signal as an excitation signal, and the input signal of SFRA is a sinusoidal wave with varying frequency, but constant amplitude. IFRA can quickly determine the transfer function of transformer windings, but due to insufficient data in the low-frequency part of the injected pulse and different frequencies of its accuracy, external interference can also affect its measurement accuracy, and the source of the pulse is more difficult to design. SFRA obtains a frequency response curve of the whole transformer winding system. The main analysis is the relationship between peak and valley and frequency, and this is compared with historical data. Therefore, the SFRA method is more accurate in the lower-frequency part than IFRA and more sensitive to the inter-turn fault response. However, due to the wide frequency of the sweep signal injected each time, it takes a long time to detect whether the winding fails each time, while improving the accuracy of evaluating the winding failure. Therefore, both offline detection methods need the transformer to cooperate with power outages or after a power outage caused by transformer failure. It is not possible to detect the running status of windings in real time and online.

In addition to the widely used offline detection methods, online detection methods have also been the focus of extensive research. The vibration analysis method [6] analyzes the operation of the winding by attaching the vibration sensor to the transformer casing and obtaining the vibration vector (spectrum signal, power spectrum, energy spectrum, etc.). However, when a transformer malfunctions, the transformer casing will induce high voltage, and sensors directly installed in the transformer casing will pose a safety hazard to testing equipment and personnel. The ultrasonic measurement method [7] is rarely reported at home and abroad. At present, it has encountered a development bottleneck in technology. This is because the sensor probe needs to be installed in the transformer to realize the measurement of the ultrasonic signal, which affects the insulation design inside the transformer. The online short-circuit impedance method [8] obtains the power frequency voltage circuit signals of the high- and low-voltage sides of the transformer through online measurement, and it calculates the short-circuit impedance value of the winding based on this signal to detect transformer faults. However, this method is not sensitive enough to capacitive winding faults. The authors of [9] introduced an online testing method for winding deformation based on pulse-coupling injection. The excitation signal is injected through a capacitive voltage divider installed on the transformer bushing, but the injected signal may affect the normal operation of the transformer, and other equipment may also be affected. In a gas-insulated switchgear (GIS) substation, switching the circuit breaker on and off will produce very-fast transient voltage (VFTO). The authors of [10] used VFTO as an excitation to detect winding deformation, but only established a centralized parameter model to verify its feasibility. For transformer winding deformation, verification was carried out by changing single parameters such as capacitance and inductance values, without corresponding to the actual deformation type. Therefore, this paper uses the finite element simulation method to analyze the causes of actual deformation faults, and further verifies the feasibility of using VFTO as an excitation to detect winding deformation.

In response to the above issues, this paper uses the VFTO signal generated by operating the isolation switch in GIS as the excitation source, impacts the transformer, and combines with the frequency response method to conduct research on online detection of transformer winding deformation based on VFTO characteristics. The internal environment of GIS equipment and the complexity of power equipment make the generated VFTO waveform large in amplitude and wide in frequency. Therefore, VFTO has the ability to detect transformer winding deformation. Due to the uncertainty of VFTO, the signal after the transformer winding is also random, which is not conducive to the analysis of

winding faults. Therefore, combined with the frequency response method, the transformer winding system is directly analyzed to obtain general rules. Another important aspect is to model the equivalent circuit of transformer windings, calculating various parameters such as inductance, inter-turn capacitance, and inter-cake capacitance before and after winding deformation. However, in fact, the analytical method has a large error, and it is difficult to calculate the electrical parameters of the faulty transformer winding, and the simulation of transformer winding faults is also complicated. A single change of a certain electrical parameter is not equivalent to a certain fault. This paper will analyze the comprehensive factors of winding faults, construct a model of winding radial deformation, axial deformation, and axis offset, set different degrees of deformation, obtain the general rules of capacitance and inductance values corresponding to different fault types and degrees, and verify the feasibility of using VFTO for winding deformation detection.

2. Fundamental

Current research shows that the magnetic permeability of an iron core is almost equivalent to that of air at higher frequencies greater than 1 kHz, so the influence of the iron core can be ignored. Therefore, the transformer winding can also be seen as a two-port network composed of C, L, and R [11–13], whose parameters are determined by the state of the winding. The parameters of the winding will change in accordance with changes in the winding state. The frequency response curve is determined by network parameters and can also reflect the transmission characteristics of a two-port network. Therefore, combining with the frequency response method can achieve detection of winding deformation. Researchers have developed three comparative methods based on frequency response and analogy, namely comprehensive analysis at different time periods (longitudinal comparison), same type analysis (horizontal comparison), and phase-to-phase analysis (lateral relative comparison). Among them, the most valuable method for fault diagnosis is comprehensive analysis at different time periods. Therefore, we will compare the frequency response curve of transformers after leaving the site with the frequency response curve after operating for a period of time. The detection principal diagram is shown in Figure 1, which applies an excitation voltage signal to one end of the winding and detects feedback information obtained from the other end of the winding. In order to obtain the frequency response curve of the transformer winding, Fourier transform was performed on the excitation signal and the response signal through Formulas (1)–(3) to achieve online measurement of transformer winding deformation.

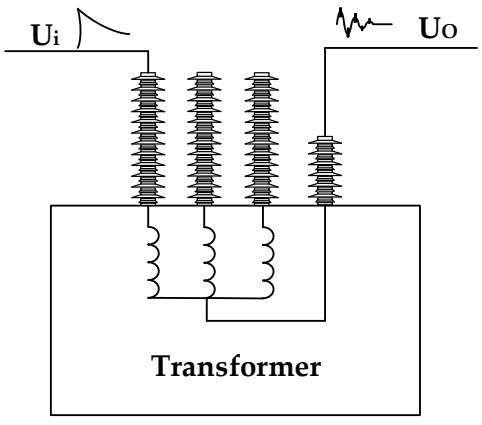

Figure 1. Detection principal diagram.

$$U_i(f) = f(U_i(t)), \tag{1}$$

$$U_o(f) = f(U_o(t)), \tag{2}$$

$$TF = 20\log_{10}\frac{|U_o(f)|}{|U_i(f)|,} \quad (3)$$

In the formula, $U_i(t)$ is the VFTO signal invading the transformer, and $U_i(f)$ is the spectral function of the VFTO signal, $U_o(t)$ is the response signal output by VFTO after passing through a certain winding of the transformer, and $U_o(f)$ is the spectral function of the signal. TF is the logarithmic amplitude gain of the frequency response of the winding.

When a fault such as deformation or short circuit occurs in the transformer winding, the parameters such as distributed capacitance, inductance, and resistance in the equivalent circuit model will change compared with the normal ones, resulting in a change in the frequency response curve of the system. According to this change of the frequency response curve, it can be judged whether the transformer winding is faulty.

3. Establishment of Transformer Winding's Equivalent Circuit Model

Transformer windings may experience various failures during transportation, under insulation degradation, and under unchangeable external disturbances such as operating environments. Especially in the case of a short circuit outside the transformer, a large amount of radial stress and axial stress will be formed due to the short-circuit current, which will deform the winding of the transformer. At the same time, the deformation will accumulate, and as the degree of deformation gradually increases, even a small short-circuit current will cause the transformer to shut down.

In this paper, a 500 kV transformer is taken as an example to establish the circuit model. The finite element software was used to calculate the corresponding circuit parameter changes under the amplitude deformation, axial deformation, and axis offset of the winding. The winding structure of the transformer is shown in Figure 2 and the relevant size parameters are shown in Table 1.

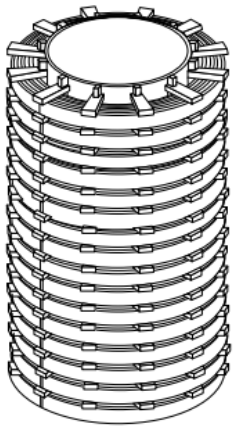

Figure 2. Winding structure of the transformer.

Table 1. Structural dimension parameters of high-voltage windings.

Parameter	Parameter Value
Number of cakes	96
Number of pads × wide	16 × 50 mm
Net metal height of conductor	9.65 mm
Internal radius of high-voltage coil	1074 mm
External radius of inner winding	1011 mm
Radial height of wire cake	348 mm
Average diameter of wire cake	1245 mm
Axial height of coil	2000 mm
Outer radius of core	600 mm
Outside radius of high-voltage coil	1740 mm

The windings consist of tortilla-like coils, in which a certain number of turns are radially bypassed before passing the next pie. Each pie is separated by a spacer, and radial pipes are created to allow oil to flow through and cool the windings. Since it is possible to have a large number of electrical turns on a smaller axis, it is commonly used in applications of high-voltage windings. At present, there are many research results on the simulation of transient circuits in transformer windings under high-frequency conditions, which can be divided into three models. The multi-conductor transmission line model regards each turn of the transformer winding as a transmission line, but this model has a large amount of calculation, and the uniform transmission line model has a large error. It is difficult to determine the parameters of the components in the hybrid model. The uniform transmission line model combines single-conductor and multi-conductor transmission lines. In addition, there is a mixed model of multi-conductor transmission lines and concentrated parameters [14–16]. The authors of [17] used Ansys Maxwell to construct a two-dimensional model of the transformer to obtain circuit parameters and constructed an equivalent circuit model of the transformer winding [17]. Referring to this model, the transformer winding is equivalent to a (passive) network composed of C, L, and R. Since the resistance of the transformer winding itself has a small impact on the distribution of resonance points, the influence of resistance on the measurement can be ignored in the subsequent fault simulation. To simplify the calculation, a seven-cake winding equivalent circuit model was established, as shown in Figure 3.

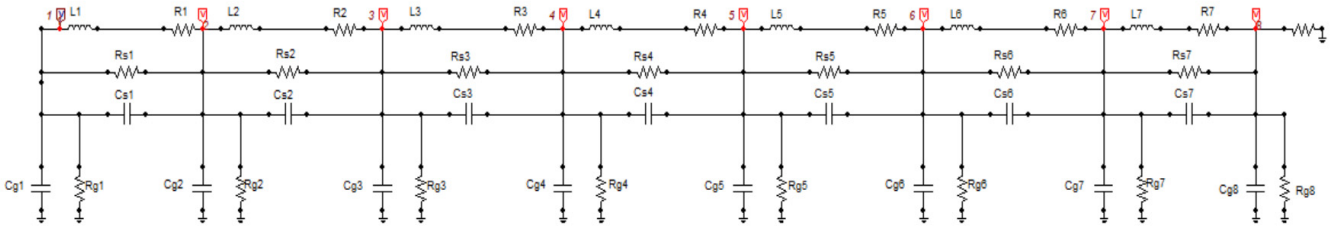

Figure 3. Equivalent circuit model of transformer windings.

The series inductance, L, and resistance, R, the longitudinal capacitance, Cs, and the resistance, Rs, the radial capacitance, Cg, and the radial resistance, Rg, which are included in each pie unit of the high-voltage side winding of the transformer, are shown in Figure 3. By measuring the VFTO signal injected into the input end of the transformer winding and the response signal output from the other end of the winding, the frequency response curve of the transformer winding can be calculated and used to analyze the transformer winding distortion.

3.1. Calculation of Equivalent Circuit Parameters of Healthy Windings

3.1.1. Inductance Value Calculation

The conductors used in power transformers are rectangular. When the current is uniformly distributed inside a rectangular geometric conductor, the inductance L of a single turn in air is given by the relationship:

$$L = 4\pi R_m(\log(\frac{8R_m}{GMD}) - 2), \quad (4)$$

wherein R_m is the average radius of the conductor and GMD is the geometric average distance of the conductor cross-section. The GMD of a rectangular conductor can be expressed using a relational expression:

$$GMD = 0.2235(H_e + W_e), \quad (5)$$

where H_e and W_e are the height and width of the conductor, respectively. Equations (4) and (5) are used to calculate the inductance of each section, except the iron core, shielding cylinder, or oil tank.

According to the geometric size of the transformer, a three-dimensional geometric model, as shown in Figure 4, was drawn in Ansys Maxwell. The material for each turn in the winding was copper, and there were 10 turns per pie. The model was simplified by omitting the edge radius of the conductor. The paper and enamel covering of the conductors had no effect on the magnetic field distribution and was, therefore, also omitted. Since no magnetic core is present, the dielectric constant of the conductor and surrounding medium was set to 1. A unit current excitation was applied to all coils in the winding, and under the static magnetic field solver, the inductance of the winding can be obtained.

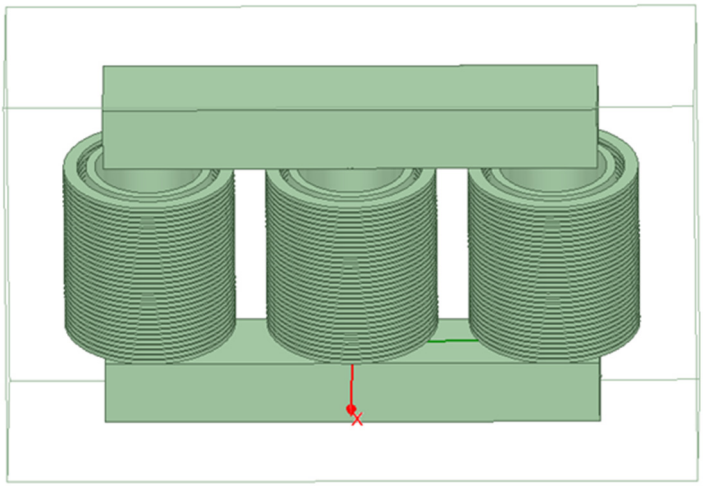

Figure 4. Three-dimensional model of transformer winding.

In the described initial setup of the 3D model of the transformer winding wire cake, a unified current was used in the calculation and generation of the inductance matrix, using the detailed, preprocessed inductance matrix generated in Ansoft Maxwell, to test the inductance finite element simulation of 10 cakes The values are shown in Table 2.

Table 2. Inductance values of windings.

Inductance	Calculated Value (uH)	Simulation Value (uH)
L1	1214.19	1259.4
L2	1693.02	1755.7
L3	1990.29	2049.1
L4	2186.77	2216.7
L5	2264.17	2294.1
L6	2265.98	2294.9
L7	2177.61	2216.4
L8	1994.12	2048.2
L9	1689.87	1754.8
L10	1211.86	1259.2

The results shown above ignore the impact of crossing. From the calculation and simulation results, it is clear that when compared with the results obtained by Ansys Maxwell, the closed Equation (4) yielded fairly accurate results. Due to the small relative error, this simulation model can be used for the simulation of winding faults.

In order to simplify the calculation model, the total inductance value of 10 wire cakes was averaged, and the equivalent inductance of each cake was calculated to be 1918.45 uH.

3.1.2. Capacitance Parameter Calculation

For the solution of the capacitance, the three-dimensional model of the transformer winding, as shown in Figure 4, was used. Capacitors in the winding structure are classified into three different types, which are referred to in this paper as longitudinal, parallel,

and ground capacitances. Figure 5 shows the equivalent capacitance distribution of the windings. Among them, the equivalent dielectric constant between turns was 2.6, the insulation dielectric constant between the wire cakes was 2.76, the equivalent dielectric constant between the high-voltage winding and the low-voltage winding was 2.42, and for the insulation between the high-voltage winding and the transformer housing, the dielectric constant was 2.2.

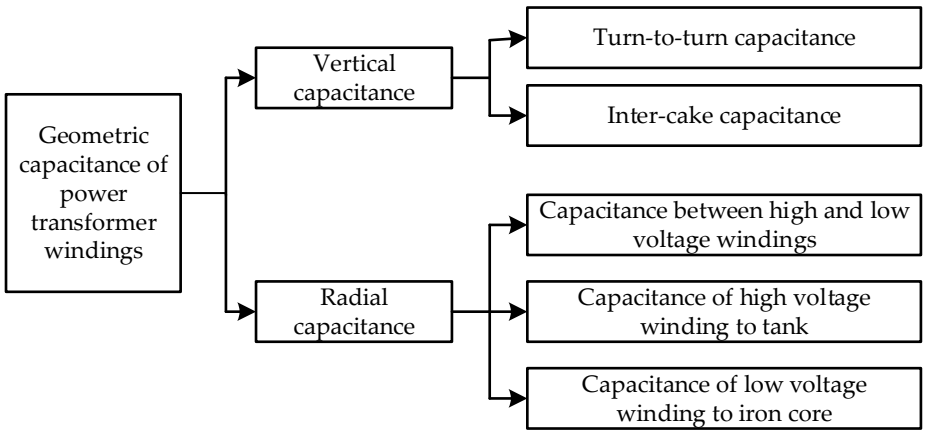

Figure 5. Equivalent capacitance distribution of transformer windings.

(1) Vertical capacitance

To calculate the total longitudinal capacitance value, two coils were taken as an example. If the coil has N turns, the added voltage excitation is U_{ds}, and the voltage between adjacent turns is U_{ds}/N, then the energy $E_w{}'$ of a single inter-turn capacitor is:

$$E_w{}' = \frac{1}{2} C_w \left(\frac{U_{ds}}{N}\right)^2, \tag{6}$$

There are $(N-2)$ inter-turn capacitances in the two coils, so the energy E_w between the two coils is:

$$E_w = (N-2)E_w{}' = C_w\left(U_{ds}^2 \frac{N-2}{2N^2}\right), \tag{7}$$

The voltage difference, $u(x)$, between turns is:

$$u(x) = U_{ds}\frac{x}{B}, \tag{8}$$

Therefore, the vertical capacitance value between the double cakes is:

$$\int_0^B \frac{1}{2}\frac{C_s}{B}\left(U_{ds}\frac{x}{B}\right)^2 dx = \frac{1}{6} C_s U_{ds}^2, \tag{9}$$

The transformer winding has many piecings, so it is necessary to consider that there is also capacitance between the two piecings and the next piecing. The formula for the total energy between the piecings is:

$$E_s = \frac{1}{3} C_s U_{ds}^2, \tag{10}$$

According to the principle of energy balance, the longitudinal capacitance between the double cakes is obtained as:

$$\frac{1}{2} C_{ds} U_{ds}^2 = E_w + E_s, \tag{11}$$

$$C_{ds} = \frac{2(E_w + E_s)}{U_{ds}^2} = \frac{N-2}{N^2}C_w + \frac{2}{3}C_s \approx \frac{C_w}{N} + \frac{2}{3}C_s, \quad (12)$$

Using the three-dimensional model of the transformer in Figure 3 and using the electrostatic solver, the partial capacitance matrix of the geometry of the test cell was obtained. A 10-fold solution area was established, and a voltage signal of 500 kV was injected into the high-voltage winding, while a voltage signal of 35 kV was injected into the low-voltage winding.

A single-wire cake with a high-voltage winding consists of 10 turns, as shown in Figure 6. By calculating the capacitance between each turn and taking its average value through the finite element method, the inter-turn capacitance of transformer windings can be obtained. The capacitance matrix of the first top pie calculated by the finite element method is shown in Table 3. The order in which the excitation is added in the finite element simulation environment is to start numbering from the first turn outside the pie, moving inwards.

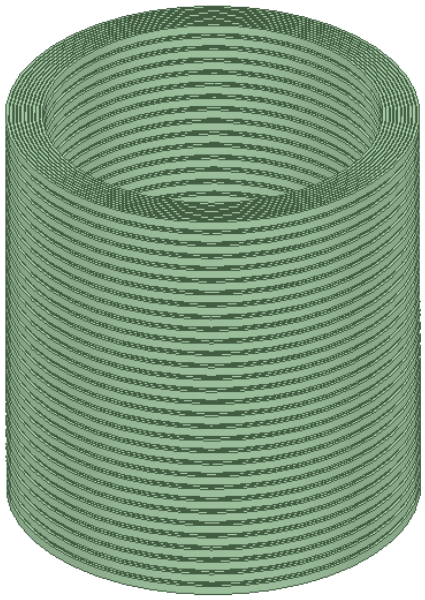

Figure 6. Transformer high-voltage winding model.

Table 3. Capacitance matrix of top first-wire pie calculated by the finite element method.

Inter-Turn Correspondence	Turn-to-Turn Capacitance (pF)
1–2	696.74
2–3	666.14
3–4	671.51
4–5	678.68
5–6	677.02
6–7	692.05
7–8	674.9
8–9	634.29
9–10	466.13

Using the finite element model of Figure 4, the capacitance between the two-wire pie was simulated and calculated. The capacitance between each turn of the two-wire pie was obtained by simulation, and the inter-pie capacitance was obtained by adding it up. The capacitance values are shown in Table 4.

Table 4. Capacitance between turns of the top two coils.

Inter-Turn Correspondence	Turn-to-Turn Capacitance (pF)
1–20	1–20
2–19	2–19
3–18	3–18
4–17	4–17
5–16	5–16
6–15	6–15
7–14	7–14
8–13	8–13
9–12	9–12
10–11	10–11

The two capacitance values obtained by the finite element software above were incorporated into the Formulas (4)–(22) to obtain an equivalent longitudinal capacitance of 1224.903 pF.

(2) Radial capacitance

The radial capacitance includes the capacitance between the high-voltage winding and the low-voltage winding, the capacitance of the high-voltage winding to the transformer shell, and the capacitance of the high-voltage winding to the iron core. Using the simulation model in Figure 4, the capacitance of each wire cake was calculated to the low-voltage winding, the shell, and the iron core, and finally, the average value was taken to obtain the radial capacitance of a single-wire cake, and the results are shown in Table 5.

Table 5. Radial capacitance of a single-wire pie.

Capacitance	Radial Capacitance (pF)
High pressure–low pressure	32.65
High voltage–transformer housing	20.62
High voltage–core	1.27
Total	54.54

3.1.3. Resistance Parameter Calculation

The formula for calculating the resistance per unit length of a transformer winding turn is as follows:

$$R = \sqrt{\pi f \mu \rho}/2(a+b), \tag{13}$$

In the formula, f is the frequency, μ is the magnetic permeability of the conductor, ρ is the resistivity of the conductor, and a and b are the lengths of the two sides of the rectangular section of the conductor.

The power lost in the dielectric is:

$$W = U^2/R = (Ed)^2 S/\rho d = \sigma E^2 S d, \tag{14}$$

In the formula, U is the voltage between turns, pie, or winding and the oil tank, d is the distance between turns, pie, or winding and the oil tank, S is the cross-sectional area of the conductor, and α is the conductivity of the conductor. Therefore, the calculation formula of longitudinal resistance and radial resistance is as follows:

$$R' = U^2/\sigma E^2 S d, \tag{15}$$

The calculation results of the resistance are shown in Table 6.

Table 6. Resistance calculation results.

Series Resistance	Longitudinal Resistance	Radial Resistance
5 mΩ	1.06 mΩ	32 mΩ

According to the above calculations, it can be concluded that the values of electrical parameters in the equivalent circuit model of healthy windings were as shown in Table 7.

Table 7. Equivalent circuit parameters of healthy windings.

Parameter	L	R	Cs	Rs	Cg	Rg
Equivalent circuit parameter values	1918.45 uH	5 mΩ	1224.903 pF	1.06 mΩ	54.54 pF	32 mΩ

3.2. Calculation of Equivalent Circuit Parameters of Deformed Windings

3.2.1. Radial Deformation

When the stress of the winding structure cannot resist the radial compressive stress, the transformer winding will warp. The deformation amount was set to 10%, 20%, and 30% of the radius. Ansys Maxwell finite element simulation software was used to establish models of different degrees of radial deformation of the windings. The high-voltage winding model with a deformation value of 10% of the radius is shown in Figure 7.

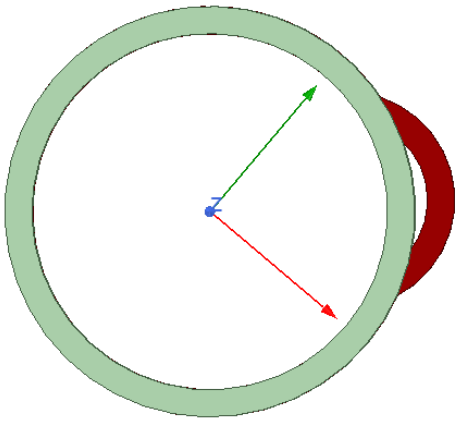

Figure 7. Top view of the high-voltage winding model with a deformation of 10% of the radius.

After the radial deformation of the high-voltage winding, the radial capacitance, longitudinal capacitance, and series inductance had changed, increased, and changed the most, respectively, causing the radial capacitance to increase with the increase in the amount of deformation. The longitudinal capacitance decreased with the increase of the deformation amount, and the series inductance value increased with the increase of the deformation amount, and the wire cake was stretched, resulting in the continuous increase of the series inductance value. The specific changes are shown in Table 8.

Table 8. Changes in circuit parameters.

	Normal winding	Deformation 10%	Deformation 20%	Deformation 30%
Radial capacitance (pF)	54.54	54.22	55.42	56.2
Vertical capacitance (pF)	1224.903	1203.17	1186.64	1164.37
Inductance value (uH)	1918.45	1923.91	1966.69	2036.28

3.2.2. Axial Deformation of Winding

If the transformer is in operation, the winding is vibrated by an axial force, which will cause friction between it and the strut, resulting in insulation damage. At the same

time, the vibration will cause the wire between each two cakes to deform. The up and down movement of the wire pie causes the spacing between the two disks of the winding to change. In severe cases, the axial deformation of the winding will cause the two wire cakes to fit together, which may cause a short circuit between the two cakes, posing a major threat to the transformer.

The Ansys Maxwell finite element simulation software was used to simulate the axial deformation of five wire cakes at the top of the transformer winding. Due to the distance between the wire cakes being 4.6 mm, the equivalent circuit parameters of 3.6 mm, 2.6 mm, and 1.6 mm were simulated.

The axial deformation of the winding mainly led to the change of the capacitance between the cakes, and indirectly led to the change of the longitudinal capacitance. The first 5 cakes were axially deformed; that is, the front view of the model with the distance between the first 5 cakes was 1.6 mm, as shown in Figure 8.

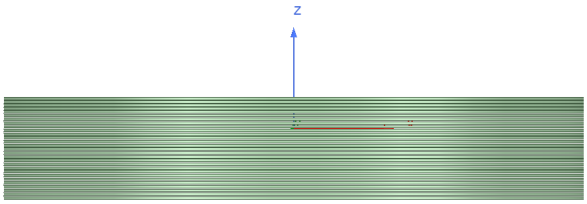

Figure 8. Front view of the model with 3.6 mm spacing between the first 5 cakes.

As the inter-cake spacing changed, the inter-cake capacitance and longitudinal capacitance changed, as shown in Table 9. It can be seen from the table that with the decrease of the distance between the cakes, the capacitance between the cakes increased, which indirectly led to the increase of the longitudinal capacitance.

Table 9. Changes in circuit parameters.

	Normal Winding	Inter-Cake Spacing, 3.6 mm	Inter-Cake Spacing, 2.6 mm	Inter-Cake Spacing, 1.6 mm
Inter-cake capacitance (pF)	1739.73	2250.9	3111.16	6606.05
Vertical capacitance value (pF)	1224.903	1565.683	2139.19	4469.17

3.2.3. Axis Offset

Through Ansys Maxwell finite element simulation software, the simulation models of 10 mm, 20 mm, and 30 mm inclinations of high-voltage winding of the transformer were established, as shown in Figure 9, which is the simulation model of the 30 mm inclination of high-voltage winding.

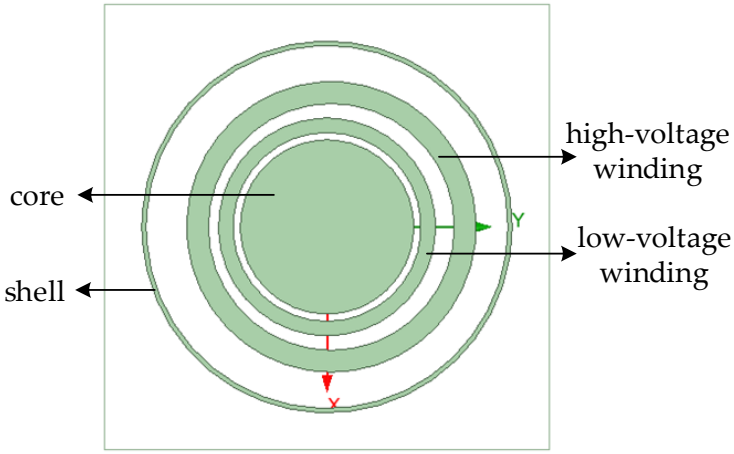

Figure 9. Top view of high-voltage winding inclined at 30 mm.

The results are shown in Table 10. As the inclination increased, the transformer winding equivalent circuit parameters, mainly radial capacitance, changed. The capacitance between the high-voltage side winding and the low-voltage side winding changed the most.

Table 10. Changes in radial capacitance values.

Capacitance	Normal Winding	Tilt 10 mm	Tilt 20 mm	Tilt 30 mm
High pressure–low pressure	32.65	42.99	48.14	53.48
High voltage–transformer housing	20.62	20.61	20.67	20.69
High voltage–core	1.27	1.2	1.19	1.18

4. Analysis of Frequency Response Characteristics Based on VFTO

4.1. VFTO Simulation Model

In the GIS substation, the root cause of VFTO is the breakdown of the contact gap caused by the voltage difference between the two ends of isolation switch contacts. The breakdown will produce VFTO, which rises along a very steep-impact voltage, and will propagate in the GIS and impact the transformer. At present, there is a lot of research and application in the VFTO simulation model and its simulation technology, and many achievements have been presented [18–21]. According to the test circuit of the isolating switch specified in IEC62271-102 and GB1985-2004, referring to the existing model, the VFTO simulation model was built using the Electro-Magnetic Transient Program (EMTP [19]), as shown in Figure 10. Among them, the simulation step size is 1 ns, and the total simulation time is 30 us.

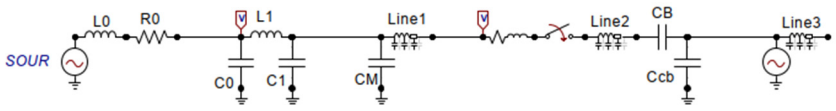

Figure 10. Simulation model of VFTO.

The VFTO waveform at the entrance of the transformer was simulated, as shown in Figure 11. Compared with the waveform analysis of the front end of the transformer injected with the medium VFTO, it was found that the step voltage range was 1.03 times the system voltage, f1 = 20.4 MHz, f2 = 3.52 MHz, f3 = 0.7326 MHz, and the frequency of the waveform safely matched with the four components of VFTO in the IEC60071-1:2006 standard. Using it as an excitation source, the actual VFTO injection into the transformer can be simulated.

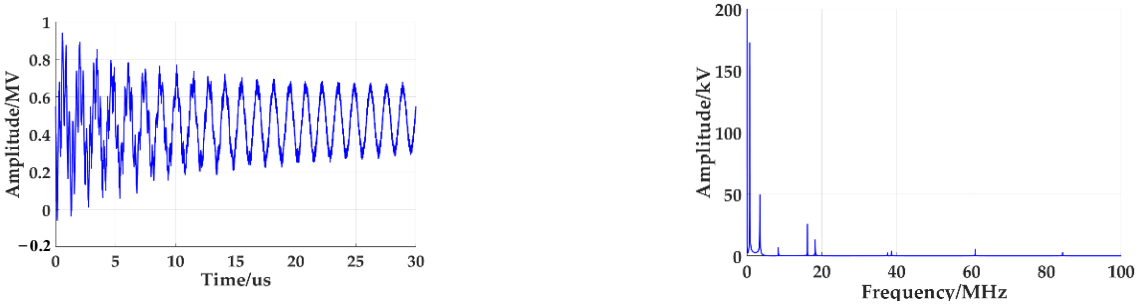

(**a**) (**b**)

Figure 11. VFTO waveform injected into the front end of the transformer. (**a**) Time domain waveform. (**b**) Spectrogram.

4.2. Healthy Winding Frequency Response Characteristics

This section describes the circuit model simulation in ATP-EMTP software, injecting VFTO signals into the established circuit model, and studying the variation characteristics of frequency response curves of windings under different deformation types and degrees. An equivalent circuit model of the transformer was established, as shown in Figure 3, in ATP-EMTP software, where the electrical parameters of each component are shown in Table 7. The VFTO waveform generated in Figure 9 was used as the excitation source. According to Formulas (1)–(3), the frequency response curve of the healthy winding was obtained, as shown in Figure 12. It can be seen that the waveform contains multiple resonance points, with alternating peaks and valleys. Among them, the horizontal axis represents the frequency, and since VFTO's frequency can reach up to 100 MHz, the range of the horizontal axis was taken up to 100 MHz, while the vertical axis represents the amplitude. Table 11 shows the frequency and amplitude of each resonance point.

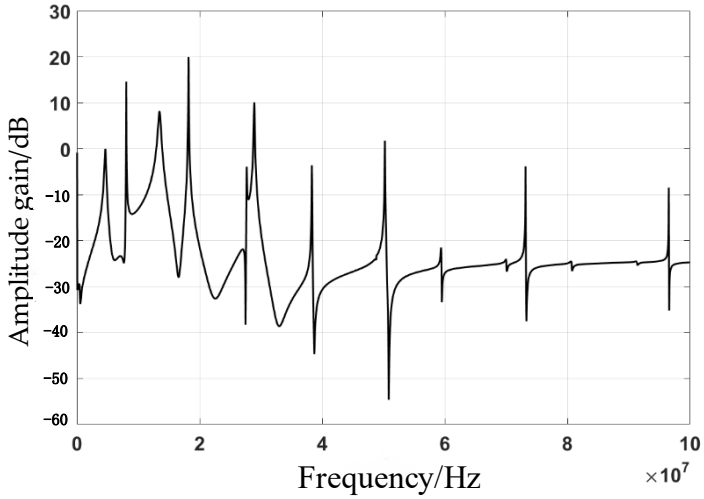

Figure 12. Frequency response curve of healthy winding.

Table 11. Frequency and amplitude of resonance points of healthy winding.

	First Resonance Point		**Second Resonance Point**		**Third Resonance Point**	
	Trough	**Crest**	**Trough**	**Crest**	**Trough**	**Crest**
Frequency/MHz	7.66		4.6		22.43	
Amplitude gain/dB	−24.82		−0.04389		−32.58	
	Fourth Resonance point		Fifth Resonance Point		Sixth Resonance Point	
	Trough	Crest	Trough	Crest	Trough	Crest
Frequency/MHz	50.86		50.23		73.33	
Amplitude gain/dB	−54.63		1.743		−37.58	

4.3. Deformed Winding Frequency Response Characteristics

4.3.1. Winding Radial Deformation

In Section 3.2, a simulation model of the radial deformation fault of windings was established. In order to simulate radial deformation of different degrees, the parameter changes were shown in Table 11, and the obtained frequency response curve is shown in Figure 13. Figure 13a is the full-band frequency response curve of radial deformation. It can be seen that the most important thing is that the trough has changed. Therefore, the change of the trough was mainly analyzed for the radial deformation of the winding. Figure 13b shows the distribution of peaks and valleys in the low-frequency region when the radial

deformation was 10%, 20%, and 30% of the original radius of the winding, respectively. As shown in the figure, as the deformation increased, the curve moved towards the high-frequency direction, and the larger the deformation, the greater the displacement. Figure 13c shows the troughs of the high-frequency part of the radial deformation of different degrees. This indicates that at higher frequencies, the frequency and amplitude gains of the curve remained basically unchanged.

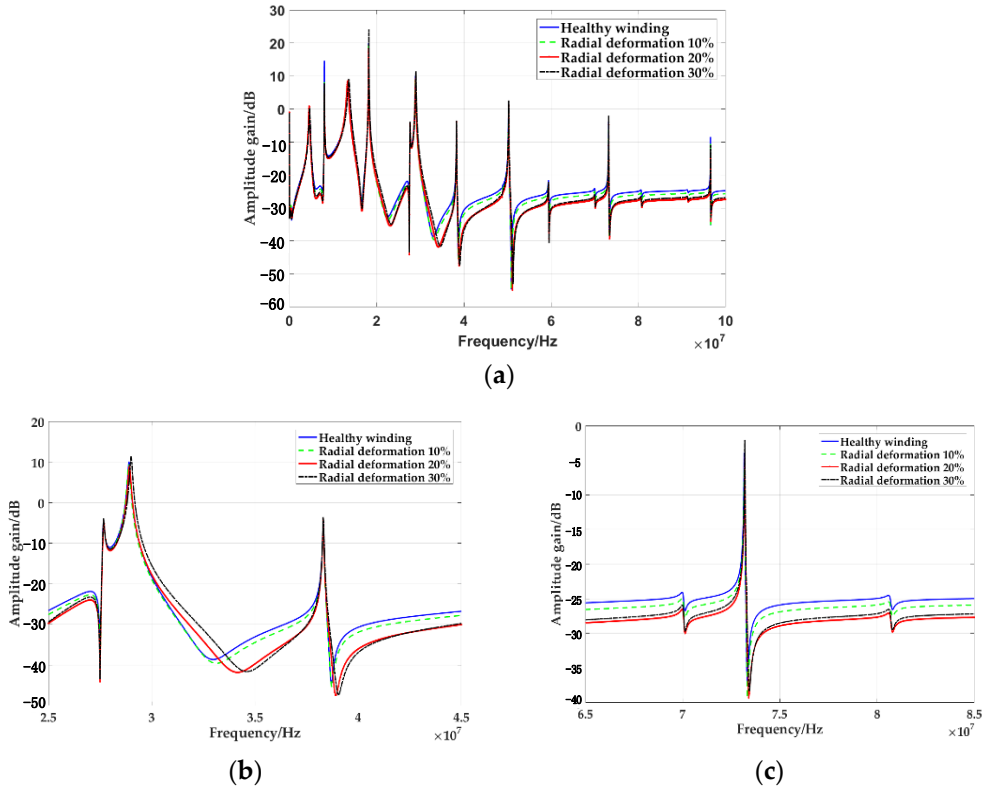

Figure 13. Frequency response curve of winding radial deformation: (**a**) full-band frequency response curve, (**b**) low-frequency partial amplification frequency response curve, and (**c**) high-frequency partial amplification frequency response curve.

According to Table 12, for a deformation of 10%, the amplitude gain of the first trough had the largest change, reaching 5.16%, the amplitude gain of the fifth trough reached 4.23%, and the frequency change of the third trough was the largest, which was 0.79%. For the deformation value of 20%, the amplitude gain of the first trough had the largest change, reaching 12.09%, and the frequency change of the third trough was the largest, which was 3.83%. For the deformation variable of 30%, the amplitude gain of the first trough was the largest, reaching 14.87%, and the frequency change of the third trough was the largest, which was 5.17%. Therefore, as the degree of radial deformation increased, the frequency value of the trough increased, and the radial deformation of the winding had a significant impact on the trough frequency and amplitude gain of medium and low frequencies, while it had little effect on the trough frequency and amplitude gain of higher frequency ranges.

4.3.2. Axial Deformation of Winding

It is known from the preceding section that the axial distortion of the winding will result in a decrease in the spacing between the pies, thus indirectly increasing the capacitance between the pies and the longitudinal capacitance. To obtain the frequency response curves with varying degrees of axial distortion, the equivalent circuit parameters of the windings were changed according to the longitudinal capacitance changes shown in Table 9, and the results are shown in Figure 14. Figure 14a is a full-band frequency response curve for axial deformation. It can be seen that the change mainly occurred in the valley. Therefore,

the main reason for the axial deformation of the winding was the change of the valley. Figure 14b is the low-frequency part of the locally amplified frequency response curve. As the degree of axial distortion increased, the trough moved toward the low-frequency direction. The larger the distortion, the greater the movement, while the frequency and amplitude gain of the peaks were basically unchanged. Figure 14c locally enlarges the high-frequency part. As the degree of axial distortion increased, the peaks moved toward the low frequency, and the valleys moved toward the high frequency, with a small amount of movement.

Table 12. Variation in valley frequency and amplitude gain.

Trough	Feature Amount	Deformation 10%	Deformation 20%	Deformation 30%
First	Frequency Variation	0	0	0
	Gain Variation	5.16%	12.09%	14.87%
Second	Frequency Variation	0.76%	2.99%	3.88%
	Gain Variation	2.95%	8.66%	7.15%
Third	Frequency Variation	0.79%	3.83%	5.17%
	Gain Variation	2.62%	8.27%	7.86%
Fourth	Frequency Variation	0.08%	0.59%	0.79%
	Gain Variation	0.24%	0.44%	−2.87%
Fifth	Frequency Variation	0.00%	0.10%	0.14%
	Gain Variation	4.23%	4.63%	2.05%
Sixth	Frequency Variation	0.00%	0.03%	0.06%
	Gain Variation	−0.20%	−3.61%	−6.16%

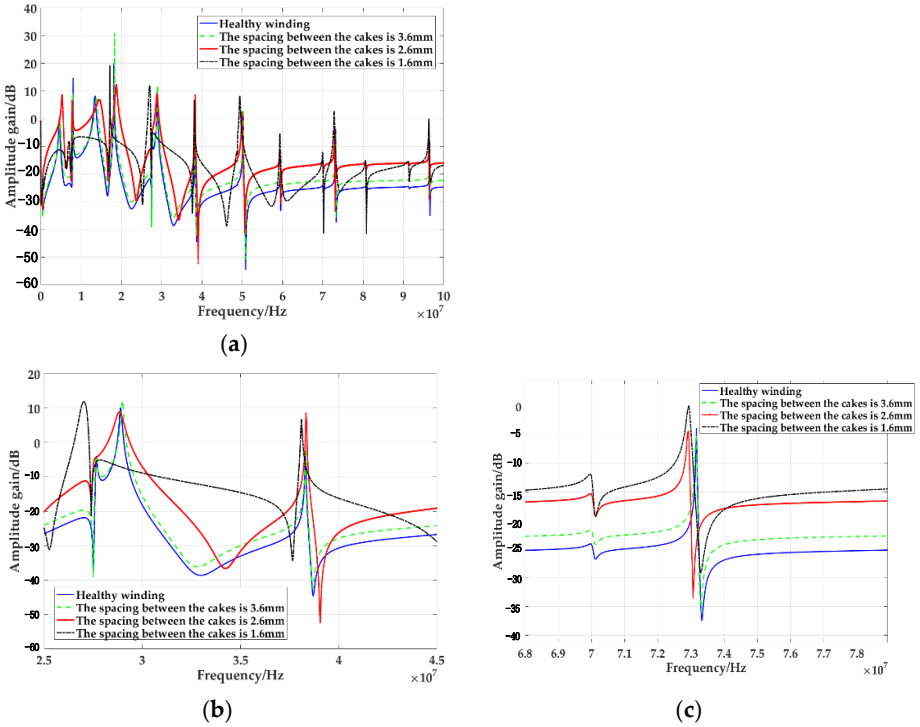

Figure 14. Frequency response curve of winding axial deformation: (**a**) full-band frequency response curve, (**b**) low-frequency partial amplification frequency response curve, and (**c**) high-frequency partial amplification frequency response curve.

Table 13 shows the variation of the valley frequency and amplitude gain of the frequency response curve. When the distance between the pies was 3.6 mm, the amplitude

gain of the sixth trough had the largest change, reaching −19.94%, and the third trough showed a maximum frequency change of −0.52%. When the distance between the pies was 2.6 mm, the amplitude gain change of the fourth trough was the largest, reaching −24.57%, and the frequency change of the second valley was the largest, which was 5.97%. When the distance between the pies was 1.6 mm, the amplitude gain variation of the sixth trough was the largest, reaching −30.93%, and the frequency variation of the third trough was the largest, which was 8.21%. Therefore, as the axial deformation deepened, the frequency of the trough increased, and the change in the amplitude gain was larger. The axial distortion of the winding had a greater impact on the trough frequency and amplitude gain in the low-frequency range, while the trough frequency was not affected in the higher frequency range, but the amplitude gain greatly changed.

Table 13. Variation in valley frequency and amplitude gain.

Trough	Feature Amount	Pie Spacing 3.6 mm	Pie Spacing 2.6 mm	Pie Spacing 1.6 mm
First	Frequency Variation	0.00%	−1.70%	−1.31%
	Gain Variation	−13.26%	−9.39%	−22.48%
Second	Frequency Variation	0.31%	5.97%	6.42%
	Gain Variation	−7.31%	−8.75%	−12.52%
Third	Frequency Variation	−0.52%	3.74%	8.21%
	Gain Variation	−6.41%	−5.86%	−4.25%
Fourth	Frequency Variation	−0.12%	−0.39%	0.87%
	Gain Variation	−6.81%	−24.57%	−29.12%
Fifth	Frequency Variation	−0.04%	−0.37%	−0.04%
	Gain Variation	−4.20%	−10.99%	−22.54%
Sixth	Frequency Variation	−0.04%	−0.21%	−0.07%
	Gain Variation	−19.94%	−17.86%	−30.93%

4.3.3. Winding Axis Offset

It was obtained from the simulation of winding axis offset in Section 3.2.3 that with the deepening of the inclination, the equivalent circuit parameters of the transformer windings have changed, and most importantly, the radial capacitance has changed. The frequency response curve of the winding axis offset can be simulated according to the radial capacitance parameters in Table 10, as shown in Figure 15. Figure 15a is the frequency response curve of the whole frequency band. It can be seen that the trough mainly changed in amplitude, and the resonant frequency of the wave crest shifted in the low-frequency part. Figure 15b enlarges the low frequency of the frequency response curve to obtain a local graph. From the graph, it can be seen that the frequency of the peak increased with the increase of the axis offset, and the larger the offset, the greater the increase, but the amplitude gain was basically unchanged. The frequency of the valley moved slightly toward the low-frequency direction, while the amplitude gain decreased. Figure 15c shows the frequency response curve of the high-frequency partial amplification. It can be seen that when the axis offset continued to increase, the frequency of the peak decreased, and the amplitude gain was basically unchanged. The frequency of the valley decreased, and the amplitude gain decreased.

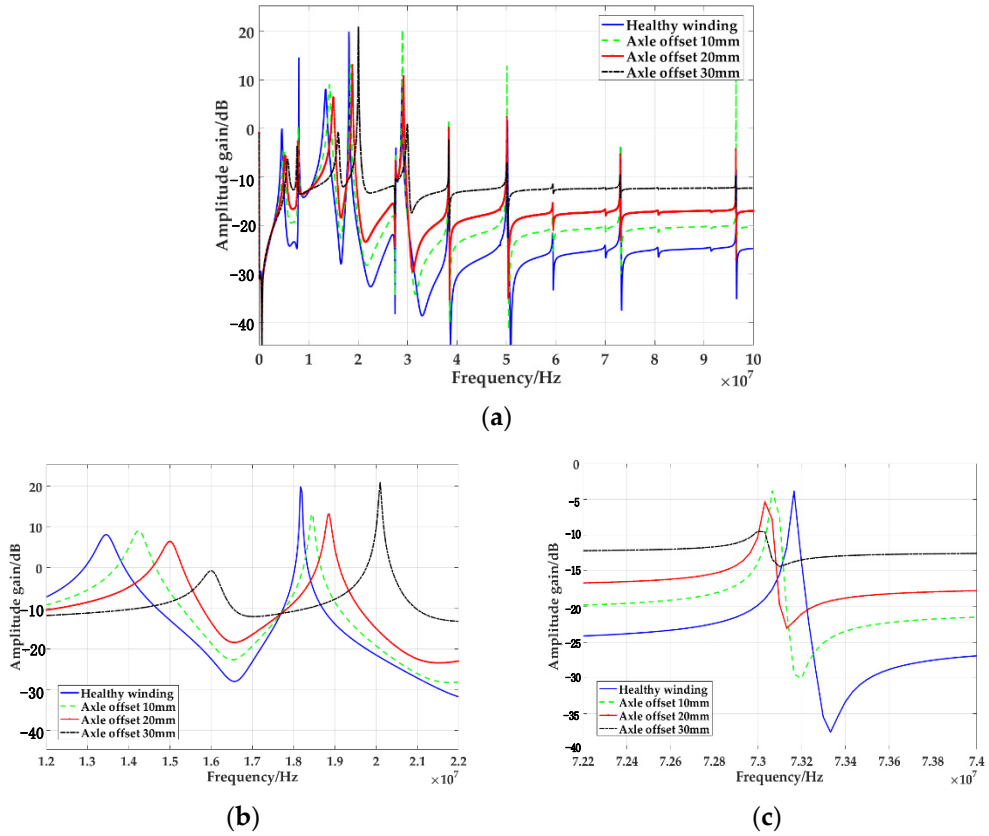

Figure 15. Frequency response curve of winding center offset: (**a**) full-band frequency response curve, (**b**) low-frequency partial amplification frequency response curve, and (**c**) high-frequency partial amplification frequency response curve.

The changes in frequency and amplitude gains of the trough and peak in the frequency response curve are shown in Tables 14 and 15. When the axis was offset by 10 mm, the amplitude gain of the sixth trough had the largest change, reaching −25.45%. The third trough had the largest frequency change, which was −4.38%. The amplitude gain change of the first-wave peak was the largest, reaching 8979.52%, and the frequency change of the first-wave peak was the largest, which was 8.7%. When the axis was offset by 20 mm, the amplitude gain of the fifth trough had the largest change, reaching −38.74%, the second trough had the largest frequency change, which was −5.04%, and the amplitude gain of the first peak has changed. The maximum amount was 12,672.84%, and the frequency change of the first peak was the largest, which was 15.22%. When the axis was offset by 30 mm, the amplitude gain of the fifth trough had the largest change, reaching −61.63%, the third trough had the largest frequency change, which was −6.69%, and the amplitude gain of the first peak has changed. The largest amount reached 14,299.64%, and the first-wave peak had the largest frequency change, which was 24.63%. Thus, in the low-frequency range, the frequency of the troughs decreased as the axis offset increased, the frequency of the peaks increased, and the magnitude gains decreased for both. The frequency of troughs and peaks in the high-frequency range decreased, and the change of amplitude gain was large for both. In addition, the winding axis offset had less effect on the frequency of troughs and peaks in the low-frequency range and more effect on the amplitude gain, while the frequency of troughs and peaks in the higher frequency range was largely unaffected, but the amplitude gain showed more change.

Table 14. Variation in valley frequency and amplitude gain.

Trough	Feature Amount	Axis Offset 10 mm	Axis Offset 20 mm	Axis Offset 30 mm
First	Frequency Variation	0.00%	0.00%	0.00%
	Gain Variation	−22.64%	−33.36%	−51.05%
Second	Frequency Variation	−3.57%	−5.04%	−3.70%
	Gain Variation	−13.60%	−28.67%	−60.80%
Third	Frequency Variation	−4.38%	−4.87%	−6.69%
	Gain Variation	−12.14%	−24.69%	−56.33%
Fourth	Frequency Variation	−0.71%	−0.90%	−1.18%
	Gain Variation	−23.80%	−35.99%	−58.67%
Fifth	Frequency Variation	−0.18%	−0.27%	−0.31%
	Gain Variation	−19.96%	−38.74%	−61.63%
Sixth	Frequency Variation	−0.10%	−0.14%	−0.18%
	Gain Variation	−25.45%	−23.37%	−53.88%

Table 15. Variation in peak frequency and amplitude gain.

Crest	Feature Amount	Axis Offset 10 mm	Axis Offset 20 mm	Axis Offset 30 mm
First	Frequency Variation	8.70%	15.22%	24.63%
	Gain Variation	8979.52%	12672.84%	14299.64%
Second	Frequency Variation	5.96%	11.69%	19.14%
	Gain Variation	12.65%	−20.28%	−109.56%
Third	Frequency Variation	0.24%	1.04%	3.70%
	Gain Variation	101.79%	6.55%	−91.64%
Fourth	Frequency Variation	−0.20%	−0.26%	−0.03%
	Gain Variation	643.55%	34.65%	−504.19%
Fifth	Frequency Variation	−0.14%	−0.18%	−0.18%
	Gain Variation	−1.12%	39.27%	148.40%
Sixth	Frequency Variation	−0.10%	−0.13%	−0.16%
	Gain Variation	66.65%	−48.97%	14.61%

4.3.4. Validation Test

In order to preliminarily verify the feasibility of this detection method, an experimental platform was built on a 10 kV transformer in the laboratory for offline testing. Using a high-voltage, pulse voltage generator to simulate the VFTO signal, and using a dual-exponential pulse signal input excitation, the input signal amplitude range was 0–2 kV, and the rise time was $t < 5$ ns. The transformer used was S11-M-80/10, with a rated capacity of 80 kVA and a rated voltage of 10,000/400 V. The wiring diagram for the experiment is shown in Figure 16.

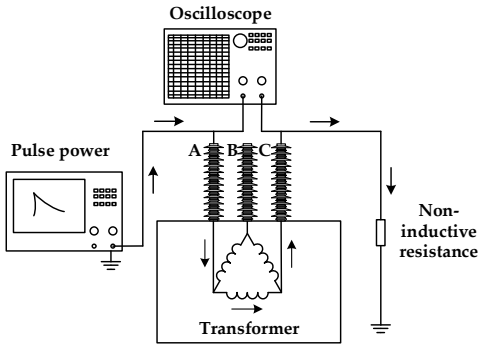

Figure 16. Experimental wiring diagram.

An experimental platform, as shown in Figure 17, was built based on the schematic diagram.

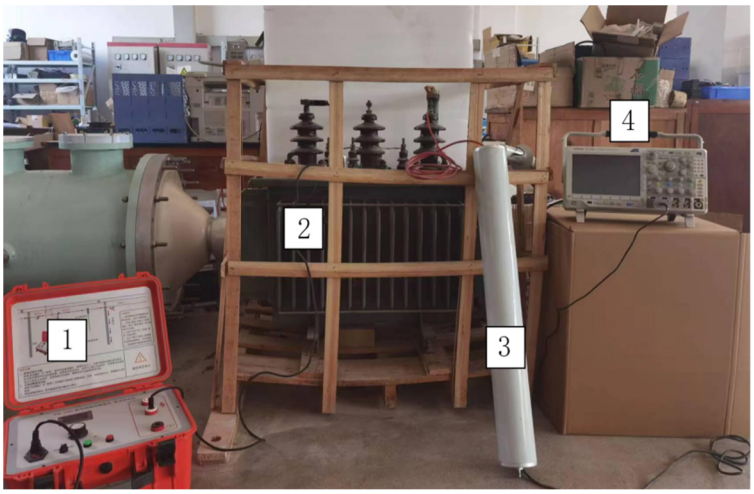

Figure 17. Experimental platform. (1) Pulse signal generation device, (2) transformer device, (3) non-inductive resistor, and (4) oscilloscope.

During the test, the pulse amplitude at the head end of the injection winding was 2 kV, the frequency was 50 Hz, and the pulse width was 200 ns. The excitation voltage signal generated by the pulse source was injected into the high-voltage phase A winding, and the signal was output from the high-voltage phase C winding. The input signal and output signal were obtained using an oscilloscope, and the results shown in Figure 18 were obtained.

The first peak frequency in the test results was 400 kHz, and the amplitude gain was −10.05 dB. The variation of the first peak frequency and amplitude gain is shown in Table 16.

Table 16. The variation of the first peak frequency and amplitude gain.

Characteristic Quantity	Series Inductance Increased by 10 μH	Series Inductance Increased by 100 μH	Series Inductance Increased by 470 μH
Frequency variation/%	30	40	45
Gain variation/%	70.95	80.8	96.71

It can be observed that when the inductance value only increased by 10 μH, the frequency increased by 35%, and the amplitude gain increased by 70.95%, indicating that small inductive faults could also be detected, confirming that this method can be used to detect transformer winding faults.

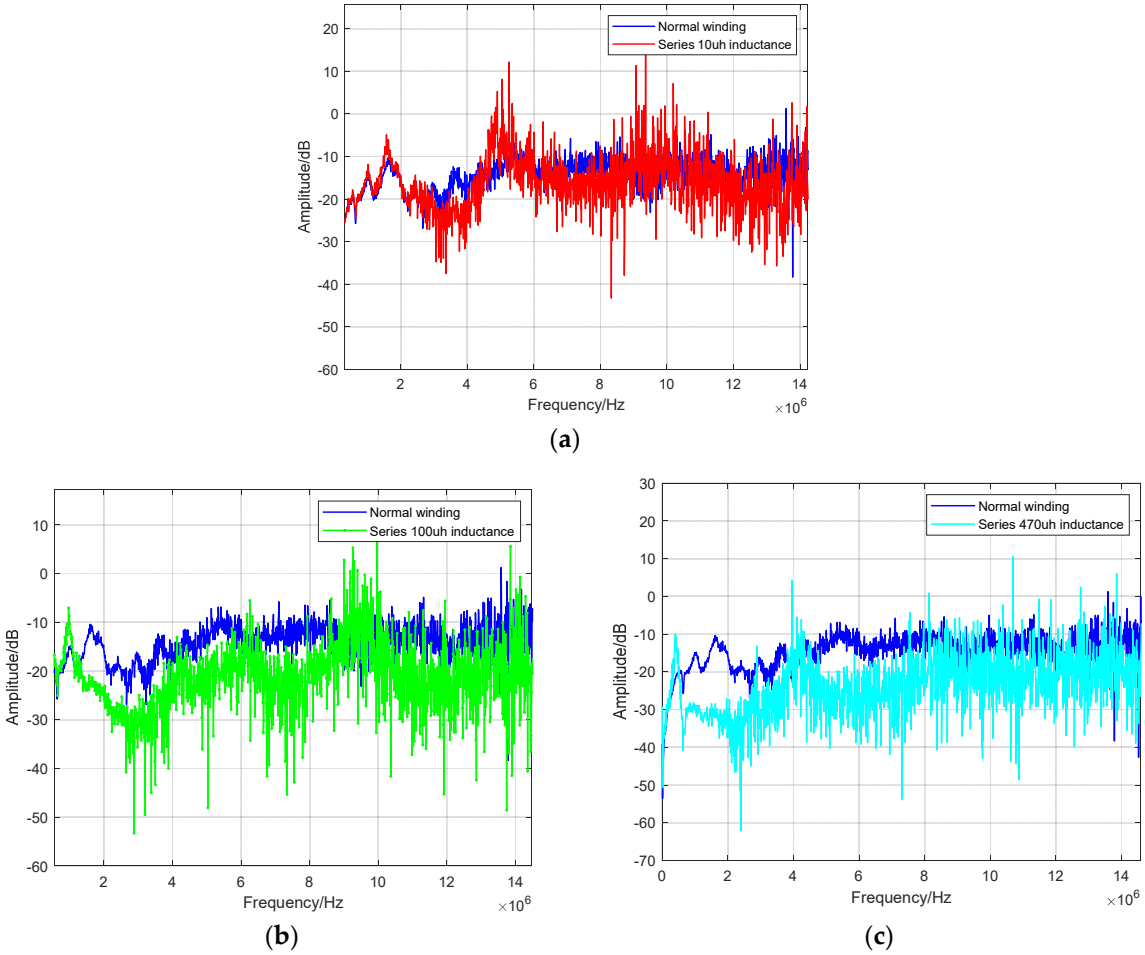

Figure 18. Experimental results. (**a**) Comparison between normal waveform and increased series inductance by 10 μH; (**b**) Comparison between normal waveform and increased series inductance by 100 μH; (**c**) Comparison between normal waveform and increased series inductance by 470 μH.

5. Discussion

According to the analysis of the simulation and experiment mentioned above, it is not difficult to find that the three types of winding deformations will undergo significant changes in the third-wave trough after injecting VFTO signals. Therefore, using the third trough data as the evaluation criterion, the main rules can be obtained as follows:

(1) The frequency value of the wave trough increased as the degree of radial deformation increased, and the winding radial deformation had a significant impact on the wave trough frequency and amplitude gain at medium and low frequencies, but it had no impact on the wave trough frequency and amplitude gain at higher frequency ranges. When the frequency variation reached above ±5% and the amplitude gain variation reached above ±15%, the transformer winding underwent a relatively high degree of radial deformation.

(2) The frequency of the wave trough increased as the axial deformation deepened, and the amplitude gain greatly changed. Among them, the axial deformation of the winding had a significant impact on the trough frequency and amplitude gain in the low-frequency range, while the trough frequency in the higher frequency range was basically not affected, but the amplitude gain greatly changed. When the frequency variation reached more than ±5% and the amplitude gain variation reached more than ±20%, the transformer winding underwent a high degree of axial deformation.

(3) The frequency of the wave trough in the low-frequency range decreased with the increase of the axis offset, and the frequency of the wave peak in the low-frequency range increased

with the increase of the axis offset. The amplitude gains of both the wave trough and the wave peak decreased with the increase of the axis offset. In the high-frequency range, both the frequency of the trough and the peak decreased as the axis offset increased, and the amplitude gain greatly changed. When the frequency variation reached more than ±5% and the amplitude gain variation reached more than ±25%, a relatively high degree of shaft center deviation occurred in the transformer winding.

Through simulation and experiments, it was verified that the offset of the resonance point of the frequency response curve can reflect the information of winding deformation, and it was proven that this method can detect small deformation of the transformer winding in a timely manner. Compared with other detection methods, it has higher security and does not affect the normal operation of the transformer, providing a new solution for transformer fault detection.

6. Conclusions

This paper verified the feasibility of online detection of transformer winding distortion using VFTO as an excitation signal. Using the VFTO simulation model in IEC62271-102 and GB1985-2004 as the excitation source, the changes of frequency response curves corresponding to different types of winding distortion were studied. This paper analyzed the reflection of different fault types and degrees on the frequency response curve and verified that VFTO can be used as an excitation to detect transformer winding deformation. The main conclusions are as follows:

(1) The equivalent circuit model of power transformer windings was established, and the circuit parameters of healthy windings and deformed windings were calculated. Each pie unit of the transformer's high-voltage side winding can be equivalent to a two-port network, composed by an inductor, a resistor, and a capacitor. The finite element software Ansys Maxwell was used to simulate the parameter values in the equivalent circuit model before and after the winding deformation.

(2) The main frequency of the VFTO before injection into the transformer was studied, and the time domain waveform and spectrogram of the VFTO were obtained by simulation. There were abundant spectral components in the VFTO waveform, mainly concentrated in the 500 kHz~20 MHz range, and its maximum amplitude could reach 1.24 pu. Its characteristics of large amplitude and a wide frequency band can be used to detect winding deformation.

(3) A VFTO detection method for transformer winding deformation based on the frequency response method was studied. By analyzing the frequency and amplitude gain information of peaks and valleys, the differences in frequency response curves of different winding deformation types can be obtained. Based on this, the frequency response curves of different degrees of deformation were analyzed and obtained. It has been proven that the peak and valley changes of the frequency response curve can reflect information on winding deformation, so VFTO can be used to detect transformer winding deformation.

The future research will focus on the following points:

(1) For the simulation of the VFTO waveform, the isolation switch test circuit specified in IEC62271-102 and GB1985-2004 was used. Although the corresponding simulation model has been built, there are certain differences between the simulation parameters and the actual waveform. Therefore, the next step is to analyze its characteristics in combination with the actual VFTO waveform before injection into the transformer.

(2) Due to the impact of the measurement on the accuracy of detecting winding deformation, the sensor for measuring VFTO will be studied in the future, and the broadband voltage sensor will also be studied to collect VFTO and response signals.

(3) Currently, only the frequency response curve has been used to analyze the change trend of different faults. The next step is to carry out research on transformer winding

fault identification technology, conduct a large number of failed winding experiments, and study fault identification methods.

Author Contributions: Conceptualization, X.S.; methodology, X.S.; software, R.W.; validation, X.S.; formal analysis, R.W.; investigation, X.S.; resources, W.Z.; data curation, R.W.; writing—original draft preparation, X.S.; writing—review and editing, R.W. and X.S.; supervision, W.Z.; project administration, W.Z. All authors have read and agreed to the published version of the manuscript.

Funding: This research was supported by the "Research and development of new smart sensor technology to promote the development of green energy" (202104BN050011) funding, and the "Scientific Research Foundation of Yunnan Provincial Department of Education" (202350134) funding.

Institutional Review Board Statement: Not applicable.

Informed Consent Statement: Not applicable.

Data Availability Statement: The data used to support the findings of this study are included within the article.

Conflicts of Interest: The authors declare no conflict of interest.

References

1. Wang, W.S.; Zhou, J.C.; Tian, Y.; Liu, H.J.; Wu, L.L.; Cheng, H.H. Simulation and Example Verification of Transformer Winding Fault Diagnosis System. *Smart Power* **2017**, *45*, 90–96.
2. Zhang, S.; Cai, Z.; Zhang, D. Online monitoring of winding deformation of power transformer based on ARM and FPGA. In Proceedings of the 2009 International Conference on Measuring Technology and Mechatronics Automation, Zhangjiajie, China, 11–12 April 2009; pp. 657–659.
3. Bagheri, M.; Naderi, M.S.; Blackburn, T. Frequency response analysis and short-circuit impedance measurement in detection of winding deformation within power transformers. *Electr. Insul. Mag.* **2013**, *29*, 33–40. [CrossRef]
4. *Guide for Reactance Method to Detect and Diagnose Winding Deformation of Power Transformer*; National Energy Administration: Beijing, China, 2018.
5. Standardization Administration of the People's Republic of China. *Power Transformer-Part 18: Measure of Frequency Response*; Standardization Administration of the People's Republic of China: Beijing, China, 2016.
6. Yu, Z.; Li, D.; Chen, L. Statistical analysis of vibration characteristics of power transformers with different voltage levels. In Proceedings of the 2018 12th International Conference on the Properties and Applications of Dielectric Materials (ICPADM), Xi'an, China, 20–24 May 2018; pp. 694–699.
7. Shu, N.Q.; Zhou, C.; Hu, F.; Liu, Q.S.; Zheng, L.W. Study on ultrasonic measurement device for transformer winding deformation. In Proceedings of the International Conference on Power System Technology, Kunming, China, 13–17 October 2002; pp. 1401–1404.
8. Wu, Y.; Gu, L.; Zhang, X.; Wang, J. An On-Line Identification Method for Short-Circuit Impedance of Transformer Winding Based on Sudden Short Circuit Test. *Lect. Notes Electr. Eng.* **2019**, *542*, 1365–1375.
9. Zhao, Z.Y. Study on Method of Detecting Power Transformer Winding Deformation Fault Based on Pulse Coupling Injection. Ph.D. Thesis, Chongqing University, Chongqing, China, 2017.
10. Wang, Y.Y.; Zhou, G.Q.; Zeng, C.P.; Zhang, W.B.; Ren, Y.N.; Ke, Y.; Chu, H.Q.; Suo, C.G. Research on On-Line Detection Method of Transformer Winding Deformation Based on VFTO. *Sensors* **2021**, *21*, 7386. [CrossRef] [PubMed]
11. Gawrylczyk, K.M.; Szymon, B. Recent Developments in the Modelling of Transformer Windings. *Energies* **2021**, *14*, 2798. [CrossRef]
12. Mao, C.; Wu, J.; Duan, W.; Han, Y.; Zhang, L.; Liu, Q.; Wang, S.; Wang, S.; Zhang, H.; Wang, S.; et al. Research of Corresponding Relationship Between Transformer Winding Deformation and Variation of Equivalent Electrical Parameters. *High Volt. Appar.* **2019**, *55*, 183–188.
13. Pham, D.A.K.; Gockenbach, E. Analysis of physical transformer circuits for frequency response interpretation and mechanical failure diagnosis. *IEEE Trans. Dielectr. Electr. Insul.* **2016**, *23*, 1491–1499. [CrossRef]
14. Wang, S.; Guo, Z.; Zhu, T.; Feng, H.K.; Wang, S.H. New Multi-conductor Transmission Line Model of Transformer Winding for Frequency Response Analysis Considering the Frequency-dependent Property of the Lamination Core. *Energies* **2018**, *11*, 826. [CrossRef]
15. Liang, G.S.; Zhang, X.L.; Wang, X.H.; Dong, H.Y.; Cui, X. Research on High-frequency Circuit Model of Transformer Windings in VFTO. *Proc. CSEE* **2006**, *26*, 144–148.
16. Ke, X.Z.; Li, Z.H. Simulation Research of VFTO Signal Coupled on Transformer Core Earthing Conductor. *High Volt. Eng.* **2021**, *47*, 3923–3931.
17. Zhou, L.; Liao, Y.F.; Luo, B.; Zhao, Z.Y.; Chen, X.H.; Yao, C.G. Simulative research on frequency response to winding deformation of power transformer based on finite element method. *Electr. Power Autom. Equip.* **2017**, *37*, 204–211.

18. Szewczyk, M.; Kutorasiński, K.; Wrońsk, M. Full-maxwell simulations of very fast transients in GIS: Case study to compare 3D and 2D-axisymmetric models of 1100 kV test set-up. *IEEE Trans. Power Deliv.* **2017**, *32*, 733–739. [CrossRef]
19. Lu, X.B.; Zhou, N.; Shi, Y.X. Effect of Arcing Model Parameter on VFTO in GIS in 3D Electromagnetic Field Simulations. *High Volt. Eng.* **2017**, *43*, 953–959.
20. Vinod, K.V.; Joy, T.M.; Naidu, M.S. Influence of switching conditions on the VFTO magnitudes in GIS. *IEEE Trans. Power Deliv.* **2001**, *16*, 539–545.
21. Schavemaker, P.H.; Sluis, L. An improved Mayr-type arc model based on current-zero measurements. *IEEE Trans. Power Deliv.* **2000**, *15*, 580–584.

Disclaimer/Publisher's Note: The statements, opinions and data contained in all publications are solely those of the individual author(s) and contributor(s) and not of MDPI and/or the editor(s). MDPI and/or the editor(s) disclaim responsibility for any injury to people or property resulting from any ideas, methods, instructions or products referred to in the content.